Asian Journal of Chemistry; Vol. 24, No. 2 (2012), 877-880

ASIAN JOURNAL OF CHEMISTRY

www.asianjournalofchemistry.co.in

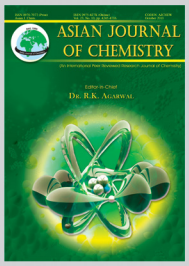

CdS Nanoparticles Embedded in Al-MCM-41 as Visible Light Photocatalysts for Hydrogen Generation from Water

SHABNAM SOHRABNEZHAD

Department of Chemistry, Faculty of Science, University of Mohaghegh Ardabili, Ardabil, Iran

Corresponding author: Fax: +98 451 5514024; Tel: +98 451 2234432; E-mail: sohrabnezhad@uma.ac.ir

(*Received*: 22 April 2011; *Accepted*: 19 October 2011) AJC-10550

Aluminum-MCM-41 molecular sieve coupled with CdS nanoparticles (CdS/Al-MCM-41) were prepared by solid-state reaction. The photocatalysts were characterized by X-ray diffraction, diffused reflectance UV-VIS (DRUV-VIS) spectroscopic analysis, scanning electron microscopic, N_2 adsorption and transmission electron microscopy. The H_2 production rate from water photocatalytic decomposition under visible light irradiation ($\lambda > 400$ nm) over CdS nanoparticles formed in Al-MCM-41 was much higher compared to the bulk CdS. The diffuse reflectance UV-visible spectra exhibited that the absorption edge was gradually blue shifted with decrease in CdS size due to the quantum confinement effect.

Key Words: CdS/Al-MCM-41, H_2 production, Photocatalysis, Diffused reflectance spectroscopy.

INTRODUCTION

Renewable new energy source has been paid more and more attention in recent years due to the exhausting fossil fuel and the world's growing demand for green energy. Hydrogen as an energy carrier may be produced from renewable energy sources *via* a variety of pathways and methods[1,2]. Some efforts have been made to fabricate hydrogen by photocatalytic degradation of organic pollutant[3-5]. Cadmium sulfide has been widely employed as a photocatalyst for production of hydrogen because of its sufficiently negative flat band potential and good absorption properties in visible light region. However, the utilization of bulk CdS has been considerably restricted due to its photocorrosion caused by exposure of it to aqueous medium under sunlight irradiation[6]. There are many attempts to overcome the photocorrosive nature of CdS. To improve its stability and activity, CdS nanoparticles were prepared and loaded on the supports with large surface area and the ability which was prone to electron transmission[7,8]. Mesoporous silica materials exhibit more suitable for loading CdS than other supports because of their several specific features such as large surface area, the concentration of reactive medium, transparency to UV-VIS radiations above 240 nm and the polarization strength of the mesoporous silica channels[9]. Hirai *et al.*[10] demonstrated that CdS nanoparticles were incorporated into modified mesoporous silica as photocatalysts for generation of H_2 by decomposition of aqueous solution of 2-propanol under UV irradiation. Guan *et al.*[11] indicated that CdS nanoparticles were assembled into titanosilicate molecular sieves as nanocom-posites for H_2 evolution in the presence of $Na_2S/Na_2SO_3/NaOH$ sacrificial donors under visible light irradiation. MCM-41 is a porous amorphous silica material with a hexagonal honeycomb structure that can be synthesized with controllable pore diameter in the range 2-10 nm. Corma[12] have reported that Al-MCM-41, with aluminum incorporated into the framework of the MCM-41, exhibited an acidity of medium strength comparable to that of US-Y zeolite. Al-MCM-41 material was used for ion exchange reaction with cations. In this work, CdS/Al-MCM-41 photocatalysts has been prepared by solid-state reaction. The photocatalyst showed high catalytic activites in photolysis of water to produce H_2.

EXPERIMENTAL

Preparation of photocatalysts: The MCM-41 and Al-MCM-41 materials were synthesized by a room temperature method with some modification in the described procedure in the literature[13]. We used tetraethylorthosilicate (TEOS, Merck, 800658) as a source of silicon and hexadecyltrimethyl-ammonium bromide (HDTMABr, BDH, 103912) as a surfactant template for preparation of the mesoporous materials. The molar composition of the reacting mixture was as follows:

$$SiO_2{:}1.6\ EA{:}0.215HDTMABr{:}325H_2O$$

EA stands for ethylamine. The MCM-41 prepared was calcined at 550 ºC for 5 h to decompose the surfactant and obtain the

white powder. This powder was used as the parent material to prepared Al-MCM-41 free surfactant materials by post-synthesis alumination method. The Al-MCM-41 surfactant-free material is white. This powder sample was used for loading the nanoparticles. The syntheses of CdS nanoparticles in Al-MCM-41 were carried out by the following method. Al-MCM-41 was mixed mechanically with $CdCl_2$ crystal. The resulting mixture was heated at 773 K for 4 h in air and then exposed to H_2S at 373 K for 1 h. The CdS particles prepared from Al-MCM-41 are described as CdS Al-MCM-41, in subsequent discussions.

For the sake of comparison, bulk CdS particles were prepared by a conventional precipitation method. In this method, an equimolar amount of Na_2S solution was added dropwise to a stirred solution of 1 M $CdCl_2$ resulting in the formation of CdS precipitates. The CdS precipitate was washed repeatedly with distilled water until free from S^{2-} ions, dried in an air-oven and then calcined at 400 ºC for 4 h in air.

Characterization: Powder X-ray diffraction patterns of the samples were recorded using a Philips X, pert diffractometer with Cu K_α radiation (λ = 1.54 Å). The UV-VIS diffused reflectance spectra obtained from UV-VIS Scinco 4100 spectrometer with an integrating sphere reflectance accessory. $BaSO_4$ was used as a reference material. The specific surface area and pore volume of the samples were measured using a sibata surface area apparatus 1100. All of the samples were first degassed at 250 ºC for 2 h. The surface morphology of the samples was obtained using a Jeol-JSM-5610 LV scanning electron microscopy. Chemical analysis of the samples was done by energy dispersive X-ray analysis. The transmission electron micrographs were recorded with a Philips EM208 microscope, working at a 100kV accelerating voltage. Samples for transmission electron micrographs were prepared by dispersing the powdered sample in acetone by sonication and then drip drying on a copper grid (400 mesh) coated with carbon film.

Evaluation of photocatalytic activity: The catalytic activity and deactivation were studied in a batch reactor. About 0.03 g of catalyst was suspended in 30 mL of an aqueous solution containing 0.02 M of sodium sulfide. The solution was kept under stirring with a magnetic stirrer, prohibiting particles to settle at the bottom of the reactor. Prior to irradiation, the reaction mixture was purged with N_2 in order to remove dissolved gases. A 300 W tungsten filament lamp was used as visible light source. The evolved gas collected by water displacement technique and was analyzed on GC (Sigma Instruments) using 5 Å molecular sieve column in TCD mode. The apparent quantum efficiency (QE) was calculated by the following formula.

$$QE = 2\frac{\text{Number of } H_2 \text{ molecules evolved}}{\text{Number of incident photons reacting surface}} \times 100\%$$

RESULTS AND DISCUSSION

Mesostructural and ordered characteristics of the samples are manifested by XRD measurement. Fig. 1 shows the XRD patterns of Al-MCM-41 host and CdS/Al-MCM-41. Three reflection peaks are detected in Al-MCM-41, which corresponds to the characteristic of MCM-41,[14] indicating the presence of long-range hexagonal ordered structure in the Al-MCM-41 host. But the CdS/Al-MCM-41 shows only one sharp reflection peak (1 0 0), which means that the mesoporous structure of Al-MCM-41 is less ordered after being loaded with CdS. Moreover, the (1 0 0) peak of CdS/Al-MCM-41 demonstrates an obvious decrease in intensity, which should be attributed to the filling of CdS nanoparticles[15]. In the region of 2θ = 10-80º, XRD pattern (Fig. 1, inset) of CdS/Al-MCM-41 matches well with that of cubic CdS. The diffraction peaks are relatively broad due to nanoscale dimensions. The estimated particle size calculated using the Scherrer equation is about 2 nm[16].

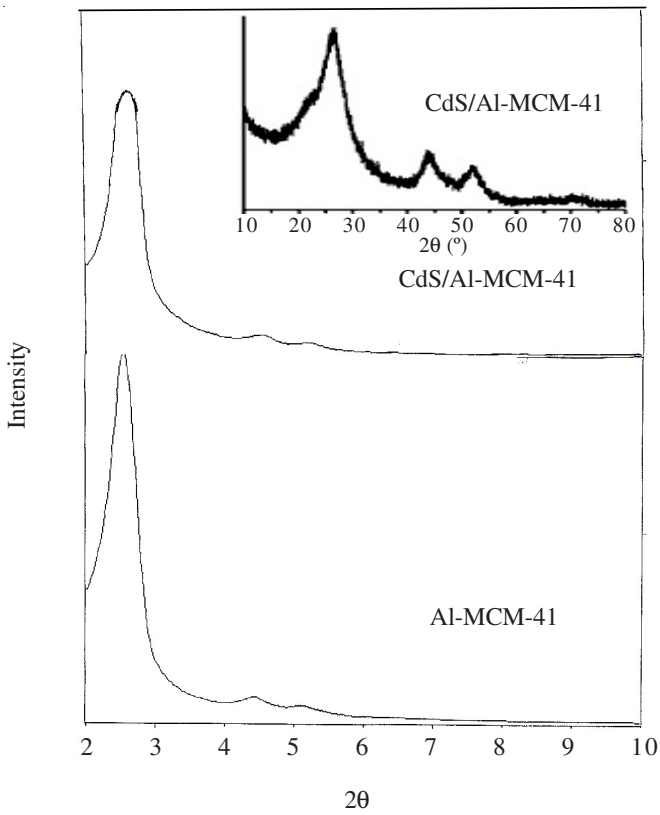

Fig. 1. X-ray diffraction patterns of samples

UV-visible absorption spectra for CdS nanoparticles prepared from Al-MCM-41 matrices, bulk CdS and Al-MCM-41 are shown in Fig. 2. The parent Al-MCM-41 [Fig. 2(c)] gave no absorption in the range 400-800 nm, while the bulk CdS [Fig. 2(a)] gave a wide absorption below 600 nm. Comparing the absorption edge of bulk CdS to that of CdS Al-MCM-41 sample prepared from mesoporous materials, it is seen that a blue shift in the onset of absorption is observed in this sample. This blue shift indicates that CdS exists as small clusters within the zeolite pores as reported by several researchers[9,17]. This was supported by a significant decrease in the surface area of CdS Al-MCM-41, compared to the parent zeolite (Table-1). This phenomenon of blue shift of absorption edge has been ascribed to a decrease in particle size. It is well known that in case of semiconductors the band gap between the valence and conduction band increases as the size of the particle decreases in the nanosize range. This results in a shift in the absorption edge to a lower wavelength region. The magnitude of the shift

depends on the particle size of the semiconductor. In the present study, the CdS Al-MCM-41 samples prepared from the Al-MCM-41 matrix showed a blue shift of *ca.* 75 nm compared to the bulk particles. From the onset of the absorption edge, the band gap of the CdS particles was calculated using the method of Tandon and Gupta[18] (Table-1). The size of CdS nanoparticles, estimated based on the results of Weller *et al.*[19] was 2 nm for CdS Al-MCM-41 sample, which is quite similar with the result of X-ray diffraction.

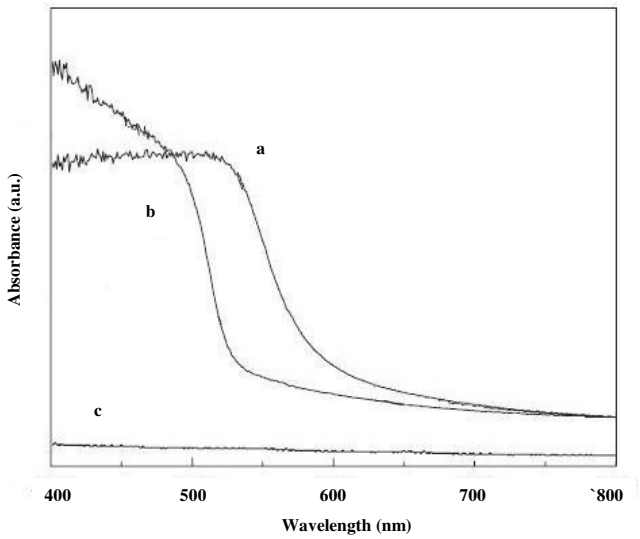

Fig. 2. UV-VIS absorption spectrum of (a) bulk CdS, (b) CdS/Al-MCM-41 and (c) Al-MCM-41

The results of the specific surface area and pore volume measurements (BET measurements) for Al-MCM-41, CdS Al-MCM-41 and bulk CdS, show that the pore volumes of the host mesoporous material, which was 0.9 mL g^{-1} for Al-MCM-41, decreased to 0.4 mL g^{-1} for CdS Al-MCM-41 materials. Similarly, the specific surface areas of the composite materials were decreased from 949 m^2 g^{-1} for Al-MCM-41 to 556 m^2 g^{-1} for CdS Al-MCM-41. Decreasing of the volumes of the pores and the specific surface area of the mesoporous material demonstrates that the guests are located in the channels (Table-1).

TABLE-1
SPECIFIC SURFACE AREA[a], PORE VOLUME[a], BAND GAP[b], PARTICLE SIZE[b], Cd/Al RATIO[c] OF SAMPLES.

Samples	Specific surface area (m^2g^{-1})	Pore volume (cm^3g^{-1})	Band gap (eV)	Particle size (nm)	Cd/Al ratio
Al-MCM-41	949	0.9	-	-	-
CdS Al-MCM-41	556	0.4	3.51	2	0.43
Bulk CdS	15	0.053	2.03	16	-

[a]Determinated by BET method, [b]See in the text,
[c]Determinated by EDX.

The surface morphology of Al-MCM-41 and CdS Al-MCM-41 is investigated by SEM and the micrographs are presented in Fig. 3. It can be seen that the crystallites of the unloaded mesoporous material, with size between 1-2 μm, have a well-defined shape [Fig. 3(a)]. There is no considerable change in morphology of CdS Al-MCM-41.

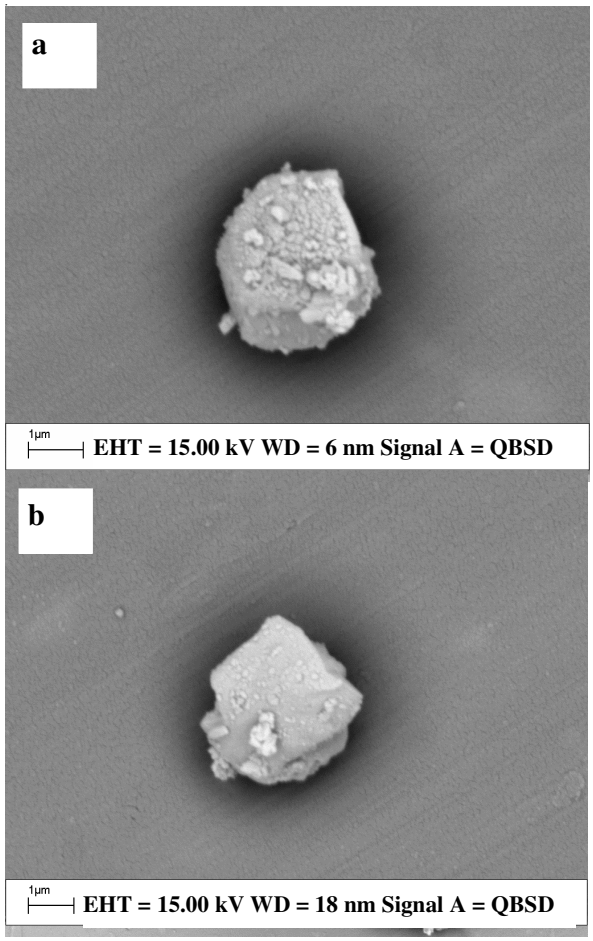

Fig. 3. Scanning electron microscopy micrographs of (a) Al-MCM-41 and (b) CdS Al-MCM-41

Transmission electron microscopy along with the textural properties of the samples discussed above bring us important information regarding whether the CdS particles are located inside or outside the pore structures used in this work. TEM images of Al-MCM-41 and CdS Al-MCM-41 samples are shown in Fig. 4(a) and (b), respectively. They were recorded under the direction parallel to the pore axis and it is possible to observe the typical Al-MCM-41 morphology in both micrographs. Although it is very difficult to identify CdS nanoparticles within the pores of MCM-41 materials by using TEM techniques[20], the higher contrast in the image of the CdS/Al-MCM-41 sample can be associated with the presence of CdS nanocrystals inside the pores of this sample.

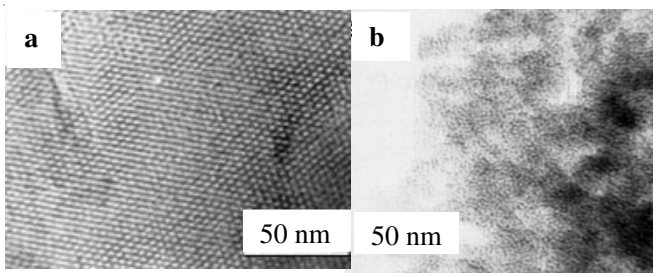

Fig. 4. Transmission electron microscopy images of (a) Al-MCM-41 and (b) CdS/Al-MCM-41

Fig. 5 shows the H_2 evolution under visible light irradiation from photolysis of water over CdS and CdS/Al-MCM-41 photocatalysis in Na_2S solution. No reaction occurred under the dark condition and without catalyst in presence of light. The evolution of hydrogen commenced after switching the lamp on in presence of catalysts only. It was seen from the graph that no H_2 evolution was observed in the Al-MCM-41 system, which shows that Al-MCM-41 itself has no photocatalytic activity for water photolysis. We studied the photocatalytic decomposition of water in the presence of CdS/Al-MCM-41, which was compared to bulk CdS. The CdS/Al-MCM-41 photocatalyst shows a higher activity compared to bulk CdS and its hydrogen evolution rate (32.8 mmol/g h) was 7.8 times higher than that of the bulk CdS (4.2 mmol/g h). This result demonstrates that high availability of CdS when it assembled inside the channels of Al-MCM-41 and Al-MCM-41 as a stable host to protect the loaded CdS particles from photocorrosion and the polarization strength of the mesoporous channels could prevent charge-recombination between electrons and holes for increasing the activity of CdS. Here, we have used sodium sulphide as sacriticial agent to evaluate the amount of H_2 liberated under visible light illumination over CdS/Al-MCM-41 because the sulphide ion (S^{2-}) is a more effective sacrificial agent than sulfite (SO_3^{2-}).[21] The scheme of photocatalytic H_2 evolution using metal sulfide semiconductors in aqueous solution containing sulphide anion can be represented by eqns. 1-3.

$$CdS/Al\text{-}MCM\text{-}41 + hv \rightarrow h^+ + e^- \quad (1)$$

$$2e^- + 2H_2O \rightarrow H_2 + 2OH^- \quad (2)$$

$$2S^{2-} + 2OH^- + 2h^+ \rightarrow S_2^{2-} + 2H^+ \quad (3)$$

The disulfide ions S_2^{2-} produced in eqn. 3 act as optical filter and compete with the reduction of proton. It can be seen from the above reaction scheme that the presence of S^{2-} anions stabilizes the catalyst surface. Moreover, in order to suppress the formation of disulphide (eqn. 3), the aqueous Na_2S and catalyst suspension was purged with N_2.

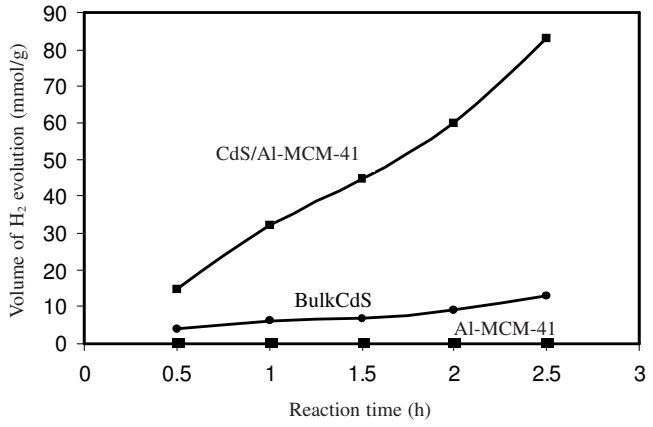

Fig. 5. H_2 evolution rate over bulk CdS, CdS/Al-MCM-41 and Al-MCM-41

Conclusion

In this paper, a simple method to synthesize CdS nanoparticles in Al-MCM-41 host have been reported. It was found from experimental results that CdS nanoparticles are inside the mesoporous materials. A blue shift in the CdS optical absorption edge is observed in the CdS/Al-MCM-41 sample with CdS nanometer crystal, as a consequence of particle size effects. The results indicated the Al-MCM-41 as a stable semiconductor matrix to protect the incorporated CdS nanoparticles from photodecomposition. The CdS/Al-MCM-41 photocatalyst shows a higher activity compared to bulk CdS and its hydrogen evolution rate (32.8 mmol/g h) was 7.8 times higher than that of the bulk CdS (4.2 mmol/g h).

REFERENCES

1. F. Barbir, *Energy*, **34**, 308 (2009).
2. M. Matsuoka, M. Kitano, M. Takeuchi, K. Tsujimaru, M. Anpo and J.M. Thomas, *Catal. Today*, **122**, 51 (2007).
3. A. Patsoura, D.I. Kondarides and X.E. Verykios, *Catal. Today*, **124**, 94 (2007).
4. A.A. Nada, M.H. Barakat, H.A. Hamed, N.R. Mohamed and T.N. Veziroglu, *Int. J. Hydrogen Energy*, **30**, 687 (2005).
5. Y. Li, G. Lu and S. Li, *Appl. Catal. A Gen.,* **214**, 179 (2001).
6. N. Buhler, K. Meier and G. Reber, *J. Phys. Chem.*, **883**, 3261 (1989).
7. S. Shen and L. Guo, *Mater. Res. Bull.*, **43**, 437 (2008).
8. S. Ryu, W. Balcerski and T. Lee, *J. Phys. Chem. C.*, **111**, 8195 (2007).
9. A. Corma and H. Garcia, *Chem. Commun.*, **40**, 1443 (2004).
10. T. Hirai and Y. Bando, *J. Colloid. Interface Sci.*, **288**, 513 (2005).
11. G. Guan, T. Kida, K. Kusakabe, K. Kimura, E. Abe and A. Yoshida, *Appl. Catal. A. Gen.*, **295**, 71 (2005).
12. A. Corma, *Chem. Rev.*, **95**, 559 (1995).
13. Q. Cai, Zh-Sh. Luo, W-Q. Pang, Y-Wei. Fan, X-H. Chen and F-Zh. Cui, *Chem. Mater.*, **13**, 258 (2001).
14. M.A. Zanjanchi and Sh. Asgari, *Solid State Ionics*, **171**, 277 (2004).
15. A. Pourahmad, Sh. Sohrabnezhad and E. Radaee, *J. Porous. Mater.*, **17**, 367 (2010).
16. B. Girginer, G. Galli, E. Chiellini and N. Bicak, *Int. J. Hydrogen Energy*, **34**, 1176 (2009).
17. W. Chen, Z. Wang and L. Lin, *J. Lumin.*, **71**, 151 (1997).
18. S.P. Tandon and G.P. Gupta, *Phys. Status. Solidii*, **38**, 363 (1970).
19. T. Vossmeyer, L. Katsikas, M. Giersig, I.G. Popovic, K. Diesner, A. Chemseddine, A. Eychmuller and H. Weller, *J. Phys. Chem.*, **98**, 7665 (1994).
20. Y.J. Zhang, L. Zhang and Sh. Li, *Int. J. Hydrogen Energy*, **35**, 438 (2010).
21. N. Zheng, X. Bu, H. Vu and P. Feng, *Angew. Chem. Int. Ed.*, **44**, 5299 (2005).